THE OFFICIAL MAGAZINE OF THE OCEANOGRAPHY SOCIETY

Oceanography

CITATION

Holland, D.M., D. Voytenko, K. Christianson, T.H. Dixon, M.J. Mei, B.R. Parizek, I. Vaňková, R.T. Walker, J.I. Walter, K. Nicholls, and D. Holland. 2016. An intensive observation of calving at Helheim Glacier, East Greenland. *Oceanography* 29(4):46–61, https://doi.org/10.5670/oceanog.2016.98.

DOI

https://doi.org/10.5670/oceanog.2016.98

An Intensive Observation of Calving at Helheim Glacier, East Greenland

By David M. Holland, Denis Voytenko, Knut Christianson, Timothy H. Dixon, M. Jeffrey Mei, Byron R. Parizek, Irena Vaňková, Ryan T. Walker, Jacob I. Walter, Keith Nicholls, and Denise Holland

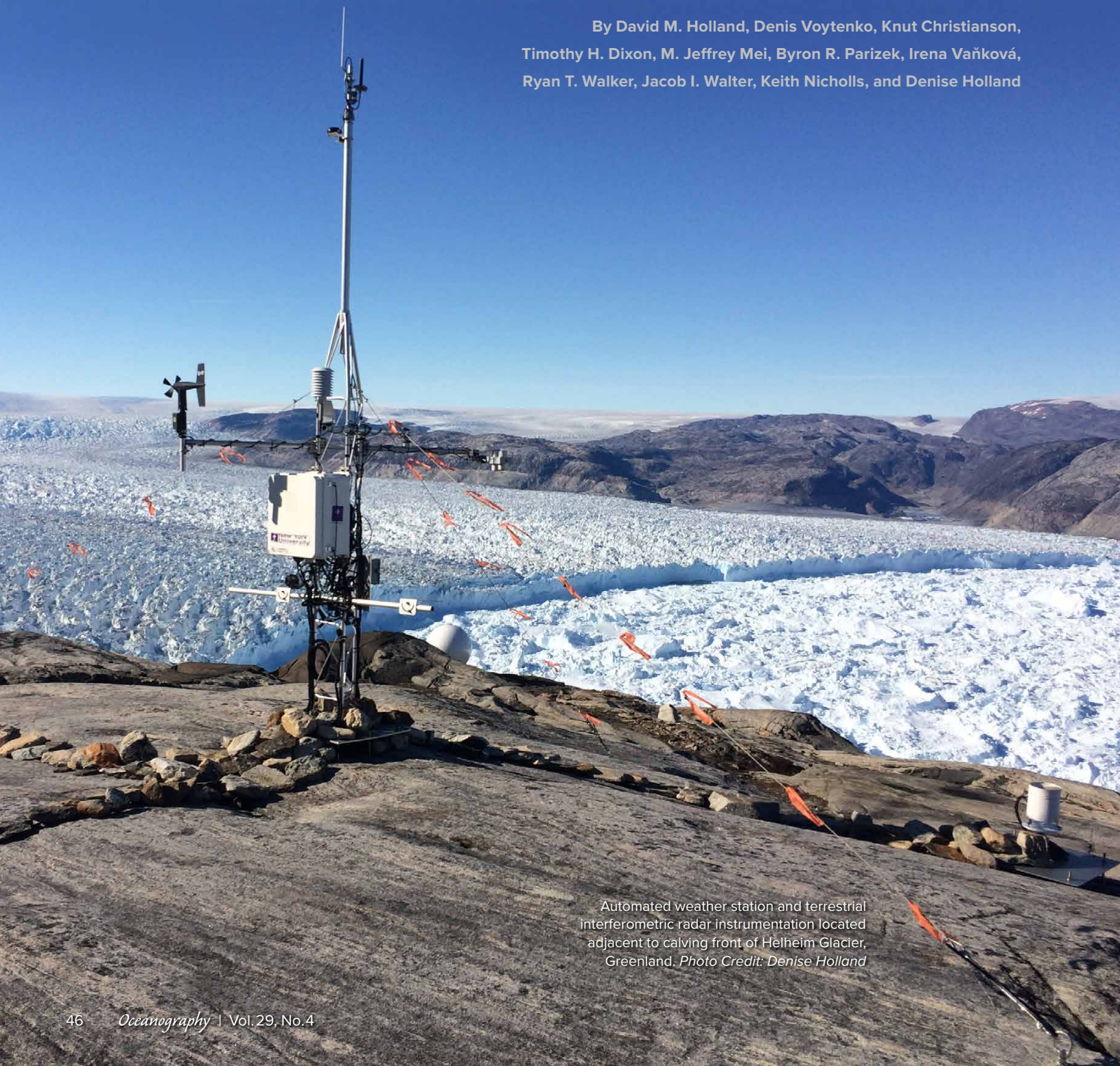

Automated weather station and terrestrial interferometric radar instrumentation located adjacent to calving front of Helheim Glacier, Greenland. *Photo Credit: Denise Holland*

> Continued development of numerical models, deterministic or probabilistic, with realistic glacier failure criteria built on rheology consistent with field observations, may ultimately lead to usable parameterizations that can make future sea level projections more robust.

ABSTRACT. Calving of glacial ice into the ocean from the Greenland Ice Sheet is an important component of global sea level rise. The calving process itself is relatively poorly observed, understood, and modeled; as such, it represents a bottleneck in improving future global sea level estimates in climate models. We organized a pilot project to observe the calving process at Helheim Glacier in East Greenland in an effort to better understand it. During an intensive one-week survey, we deployed a suite of instrumentation including a terrestrial radar interferometer, GPS receivers, seismometers, tsunameters, and an automated weather station. This effort captured a calving process and measured various glaciological, oceanographic, and atmospheric parameters before, during, and after the event. One outcome of our observations is evidence that the calving process actually consists of a number of discrete events, spread out over time, in this instance over at least two days. This time span has implications for models of the process. Realistic projections of future global sea level will depend on accurate parametrization of calving, which will require more sustained observations.

INTRODUCTION

Over the past few years, major changes along the periphery of the Greenland Ice Sheet have been observed occurring much faster than previously thought possible (Joughin et al., 2004, 2008). Glacier frontal position and velocity data, largely measured by satellite remote sensing, indicate that outlet glaciers in both East and West Greenland have retreated, thinned, and accelerated quasi-synchronously (Luckman et al., 2006; Rignot and Kanagaratnam, 2006; Moon and Joughin, 2008). These correlated responses suggest that a common thermodynamic forcing is at play. Whether an increase in air temperature (Moon and Joughin, 2008), in ocean temperature (Holland et al., 2008), or some combination of these is responsible, the mechanisms linking the forcing to subsequent dynamical retreat of the calving front, inland thinning, and acceleration remain to be resolved.

While questions about thermodynamic forcing have received significant attention, present understanding of the mechanisms controlling ice sheet dynamics is itself limited. As a consequence, projecting the magnitude of sea level rise associated with possible retreat of the Greenland Ice Sheet remains challenging. The latest Intergovernmental Panel on Climate Change Assessment Reports (IPCC, 2007, 2013) acknowledge that key glacier processes are not well understood, limiting ability to accurately project sea level rise (Joughin et al., 2012). Grounding line dynamics (Schoof, 2007), basal drag (Vaughan and Arthern, 2007), and iceberg calving (Benn et al., 2007) are among the crucial processes that now require intensive investigation. Currently, limited knowledge of these processes is an inherent reflection of their complexity and the difficulty of making field measurements, which can be both costly and hazardous. Calving of icebergs is an important component of the negative mass budget of the Greenland Ice Sheet (Benn et al., 2007). It can be argued that calving is the least understood of these processes, while at the same time probably the most critical to understanding ice sheet retreat (DeConto and Pollard, 2016).

We focused on the calving process for a typical Greenland outlet glacier, in particular one now in retreat and without a floating ice tongue, a so-called tidewater glacier. A characteristic of the calving process there, as we will demonstrate, is that it occurs over a period of at least a few days, consisting of a sequence of events during which mechanical failure of the glacier occurs. There can be precursor events during which fracture occurs in the glacier, days, hours, or minutes before the primary calving event. During the primary event, failure results in the production of a large iceberg that separates from the glacier and enters the ocean. Secondary events during which additional icebergs are calved can follow hours or days later. All of these events occur on time scales of minutes, but are spread out from one another over minutes to days. While remote sensing has revolutionized the field of glaciology, providing

unprecedented observations and insights, it nonetheless suffers a shortcoming in the context of understanding the calving process. Specifically, high-frequency repeat observations are not possible. To circumvent this shortcoming, we put together a comprehensive plan of on-the-ground, on-the-glacier, and in-the-ocean instrumentation to be deployed at the calving front of a Greenland tidewater glacier. We caution that our observations are from a single glacier, and may not generalize to others.

We sought to answer the following questions:

- How does the strain (rate) field evolve during calving?
- Does calving lead to acceleration of the glacier?
- Is there a relation between calving and cliff height?
- Or between calving and water depth?
- Can seismic signals from a close-array locate a calving event?
- Does atmospheric variability play a role in calving?
- Do ocean waves trigger calving?

Based on scientific and logistical considerations, we chose Helheim Glacier in East Greenland as our study site (Figure 1). The observations we report and the conclusions we draw represent a pilot effort that essentially demonstrates the utility of combining certain glaciological, oceanographic, and meteorological observations relevant to the calving process. Most importantly, our pilot effort demonstrates the potential for a deeper understanding of calving to be achieved through future similar, sustained in situ observations.

The next section of this article reviews existing calving theories and parameterizations and how they motivate our fieldwork. The fieldwork section describes our instrumentation and presents our key observations. The final section summarizes our findings and points to future field and modeling activities related to calving.

EXISTING CALVING PARAMETERIZATIONS

The overarching goal of our work is to develop a viable parametrization of calving that can be used in global climate models to better project sea level change arising from Greenland mass loss. A simple, universal calving law might be illusory, and many different calving mechanisms likely exist (Van der Veen, 2002; Benn et al., 2007; Vieli and Nick, 2011). To aid the reader in understanding the current state of the art in calving models, we provide some background on current theory, and how various existing parameterizations bear on the types of observations we undertake. Of course, not all physical variables are easily observable, particularly those at depth in the glacier, and this limits to some degree our field observation possibilities. A number of mechanisms discussed in the literature as triggers for glacier front calving (Figure 2), are presented below. Calving may be dominated by any one of these mechanisms, or a combination, or by mechanisms yet not envisaged.

The interaction of calving with the motion of the glacier itself is intricate, and raises the question: does calving cause change in the glacier flow field, vice versa, or both? Some researchers point out that calving leads to a reduction in the backstress and therefore an acceleration of the glacier, considered over many calving events (De Angelis and Skvarca, 2003; Howat et al., 2005). On the scale of individual calving events, this also appears to be the case (Amundson et al., 2008; Nettles et al., 2008). A contrasting view is that calving is a consequence of changes in glacier motion (Van der Veen, 2002). Computer simulations of Helheim Glacier (Nick et al., 2009) and a force balance analysis (Howat et al., 2005) suggest that the recently observed glacier acceleration, thinning, and retreat originate at the calving terminus and then propagate upstream due to changes in geometry and driving stress. These findings motivate us to observe motions at the calving front, and to ascertain if changes further upstream occur before or after calving.

Calving and associated glacial earthquakes have been previously observed at Helheim Glacier. Nettles et al. (2008) deployed a dozen GPS receivers spanning an along-flow distance of about 20 km. They also used the Global Seismographic Network to monitor glacial earthquakes, and the calving front position was estimated based on remote-sensing images. Their data show abrupt increases in the along-flow velocity that correlate well with the times of calving and glacial earthquakes. A more recent study focused on

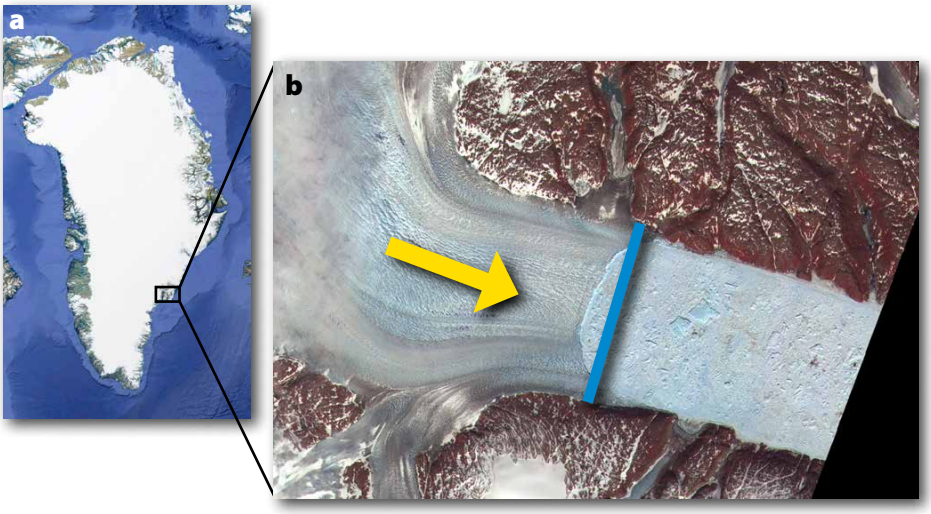

FIGURE 1. (a) Google Earth image of Greenland with the study area, Helheim Glacier, indicated by the small black box. (b) A zoomed view of the study area, showing Helheim Glacier (center left), the calving front (center), and the ice-mélange-covered ocean fjord (center right). Glacier flow direction is indicated by the yellow arrow, and the blue line marks the calving front.

glacial earthquakes at Jakobshavn Glacier on the west coast of Greenland. Sergeant et al. (2016) used broadband seismometers to invert for the force history of the calving glacier on the solid Earth. Their analysis shows that seismic data provide a unique dynamical constraint that may in the future be helpful for discriminating between different mechanical models of calving events and for quantifying associated rheological parameters. These seismic observations, along with others taken by Bartholomaus et al. (2015) relating to seismic activity brought on by subglacial discharge, inspire us to include a broadband seismic array deployed near the calving front to more precisely locate calving events.

Glacier calving is thought to be a consequence of critical failure stress in the glacier. A glacier's stress field is often modeled as being proportional to the strain rate field, influenced by nonlinear viscosity. Thus, the stretching rate of a glacier is another putative precursor to calving. Longitudinal stretching in the along-flow horizontal direction (Benn et al., 2007; Alley et al., 2008; Amundson and Truffer, 2010), if it reaches a critical strain rate (Pralong and Funk, 2005), can lead to ice failure and calving. Longitudinal stretching in both horizontal directions (Levermann et al., 2012) has also been considered. Benn et al. (2007) argue that the longitudinal strain rate is the first-order control as it determines crevasse depth, with crevassing viewed as a precursor to calving. Parameterization of calving based on longitudinal strain rate has been implemented in a two-dimensional ice-flow model (Nick et al., 2010) and a three-dimensional full-Stokes model (Otero et al., 2010). Nick et al. (2010) indicate that this parameterization produces a seasonal cycle that compares well with observations, but also point out that details relating to choice of calving criterion can affect the result. Other researchers have considered including damage mechanics, in addition to linear strain and elastic mechanics, to arrive at a calving model (Krug et al., 2014). Newly available radar instrumentation (terrestrial radar interferometry, or TRI, described below) allows us to make rapid repeat observations of glacier displacements, in turn allowing velocity and strain rate estimates over the entire front of Helheim Glacier.

Researchers have proposed empirical relations for calving that involve a single parameter, such as water depth (Brown et al., 1982). In a similar fashion, height-above-buoyancy, in which the ice thickness at the terminus is assumed to reach only a maximum or critical height-above-buoyancy (Meier and Post, 1987; Bassis and Walker, 2011), has also been proposed. However, these relationships can vary between glaciers and can even change with time for a single glacier (Van der Veen, 2002). Additionally, we must consider the possibility that a flotation criterion (i.e., a combination of water depth and cliff height) may play an important role in calving. With that caveat notwithstanding, we observe water depth and height-above-buoyancy evolution to ascertain their potential relevance to calving.

Researchers have also questioned whether or not ocean waves in the fjords abutting the glacier front play a role in calving (MacAyeal et al., 2009). Nettles et al. (2008) reported that small tsunamis followed the glacial earthquakes, and attributed them to large pieces of ice falling into the fjord during calving. In contrast, and not necessarily in contradiction, there is also evidence to suggest ocean swell triggers glacier calving (Bromirski et al., 2010). Ocean tides certainly have an impact on the motion of the glacier near the calving front, as observed using TRI (Voytenko et al., 2015b), but whether or not they play an important role in calving is not yet clear. To gain some insight into the role of ocean tsunamis and ocean tides on calving, we deployed an array of seafloor high-sampling-frequency pressure meters (i.e., tsunameters) not far from the glacier front.

A physical feature that may play a role in calving is the mélange of sea ice and icebergs that exists seaward of the calving front. The mélange may have sufficient mechanical strength to hold back the glacier front and thus influence calving, as appears to be the case on seasonal time scales at different glaciers in western

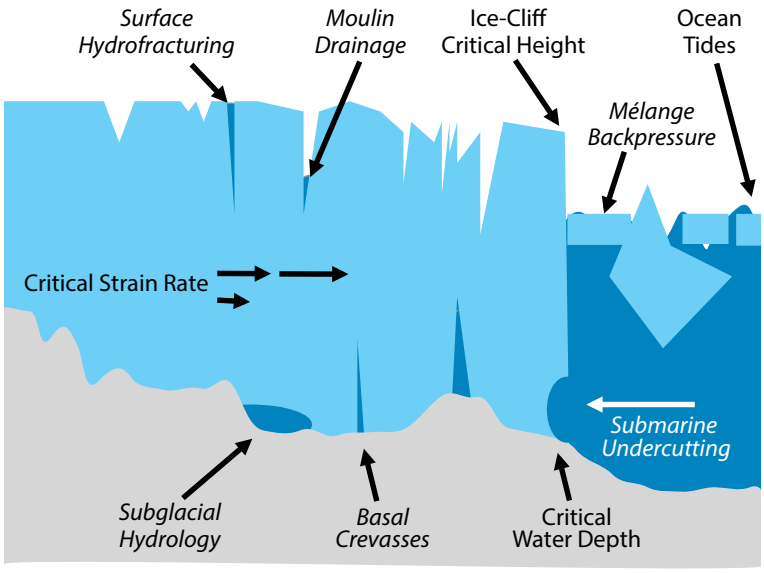

FIGURE 2. Schematic of physical mechanisms considered in existing calving parameterizations, or to be considered in the future. The mechanisms are discussed in the text. See also Van der Veen (2002), Benn et al. (2007), and Vieli and Nick (2011) for an overview of calving mechanisms. Other factors likely contribute to calving in addition to those described here. The field campaign described in this article was designed to observe as many physical quantities as possible relevant to these mechanisms in order to help elucidate the underlying physics. In this campaign, surface features were relatively straightforward to observe, while subsurface mechanisms involving subglacial hydrology, basal crevasses, and ocean-melt undercutting were not observed and remain challenging with existing instrumental capabilities. The processes not directly observed are presented in italics in the figure.

Greenland (Amundson et al., 2010; Walter et al., 2012). When Amundson et al. (2010) deployed cameras, GPS, seismometers (on bedrock), audio recorders, and water pressure sensors near the calving front of Jakobshavn, another Greenland outlet glacier, they observed large increases in the velocity of the mélange at the onset of calving events. Before a calving event, the mélange advanced at 40 meters per day, but it reached much higher speeds for several minutes during a calving event. Peters et al. (2015) used a TRI to investigate the behavior of the mélange during calving, and Voytenko et al. (2015b) described the use of near-field TRI observations to measure tidal fluctuations. Our field campaign correspondingly includes TRI observations of the mélange in front of Helheim.

Crevassing is an important precursor to calving. Colgan et al. (2016) present an extensive review of the formation of crevasses, including basal crevasses and hydrofracturing. Observations of calving at Helheim Glacier using stereo photogrammetry suggest that a basal crevasse may be a key ingredient in establishing the onset and location of calving (James et al., 2014). Murray et al. (2015) also found basal crevassing to be a likely precursor to calving at Helheim Glacier. TRI observations at Jakobshavn Glacier in West Greenland came to a similar conclusion (Xie et al., 2016). These studies point out that undercutting of the glacier front by ocean melt might lead to weakening of basal ice, and may, with buoyant flexure, force the opening of basal crevasses. No direct observations of this process have been made, and they remain extremely challenging.

Another possible driver of the calving process may be subaqueous, ocean-driven melting at the terminus. Truffer and Motyka (2016) provide a review of the relevance of this process. It is possible that mechanical calving is a passive reaction to ocean-driven melt (O'Leary and Christofferson, 2013). Subaqueous melting is difficult to observe, and is not included in the current suite of observations, but will hopefully be included in future campaigns.

Surface or near-surface meltwater may be a preconditioner for calving disintegration of an ice shelf, with hydrofracturing as a possible mechanism (Scambos et al., 2009). Recent simulations of Antarctic change have invoked hydrofracturing (DeConto and Pollard, 2016). The underlying physics is the fact that water is denser than ice, and a buildup of water in surface crevasses can lead to a catastrophic failure of the ice through pressure. For an outlet glacier such as Helheim, with a heavily crevassed surface, it may be more appropriate to consider calving as related to water-filled crevasses (Benn et al., 2007). We use an automated weather station (AWS) to record glacier surface temperature, and photos of the glacier surface to attempt to evaluate the role of surface hydrofracturing in calving.

To make a meaningful projection of outlet glacier change, Nick et al. (2010) conclude that "a realistic parameterization for the process of calving is crucial." We argue that a comprehensive observational database of calving is needed for any such parameterization. There are likely to be different types of calving, and only through observation of many calving events at many different outlet glaciers will a comprehensive understanding emerge. In the next section, we describe in detail the instrumentation we deploy to observe calving, and its arrangement near the Helheim calving front. While our pilot deployment was for a relatively short period of time, capturing a single calving event, we suggest that sustained observations and the creation of a large, publicly accessible database of many calving events could lead to a realistic and usable parameterization of calving for Greenland tidewater glaciers.

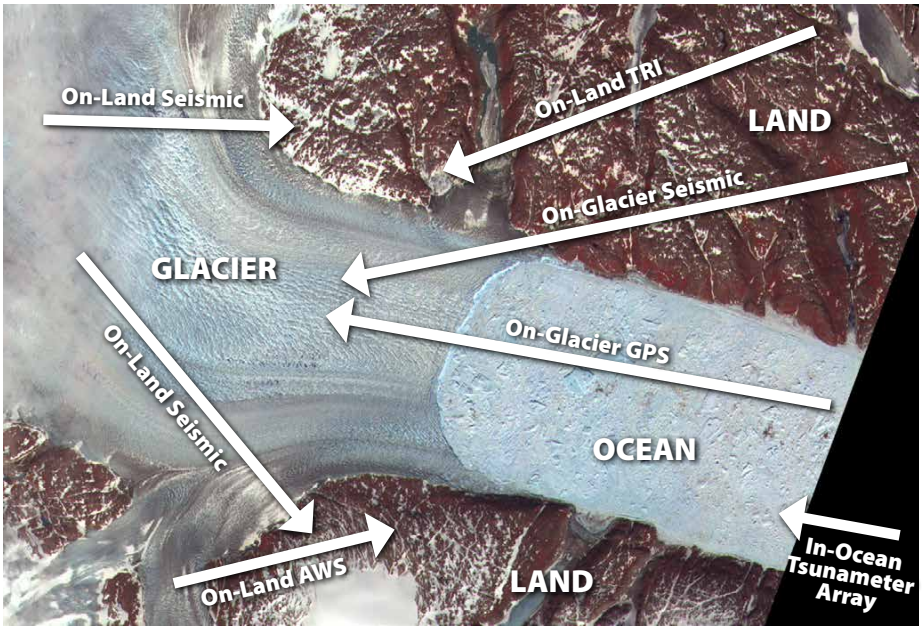

FIGURE 3. Approximate deployment locations of field instrumentation against a background image from Google Earth. Land-based instruments included a terrestrial radar interferometer (TRI), an automated weather station (AWS), and two broadband seismometers. On the glacier, several GPS and broadband seismometers were positioned along a flow line. In the ocean, a tsunameter array was installed in the adjacent Sermilik Fjord (out of picture).

FIELD CAMPAIGN

During a one-week period in August 2014, we deployed a suite of in situ instrumentation (Figures 3 and 4) to observe glacier behavior before, during, and after a calving event. The instrumentation included a TRI, broadband seismometers, and an AWS on land; GPS receivers and seismometers on the ice; and an in-ocean tsunameter array. We were fortunate that a major calving

event occurred during our one-week observational period.

The TRI mapped the evolution of the displacement field of the glacier surface and its elevation both upstream of the front and downstream over the mélange at two-minute intervals over the entire week. The on-ice GPS instruments recorded three-dimensional motion of the glacier along a flow band. We simultaneously observed seismic activity in the glacier from a set of broadband seismometers that were collocated on the glacier with the GPS, as well as from two additional broadband seismometers located on the land adjacent to the calving front. Ocean wave disturbances in the adjacent fjord were monitored from a nearby tsunameter array. Finally, we visually recorded calving events using a time-lapse camera located at the nearby AWS, which recorded temperature, humidity, solar and infrared radiation, and wind.

TRI Background

The TRI is the centerpiece of our field instrumentation. Caduff et al. (2015) review the TRI technique, and glaciological applications are discussed in Werner et al. (2008), Riesen et al. (2011), and Voytenko et al. (2015a). We first used TRI at Helheim Glacier during August 2013 to observe tidal variability of the glacier front velocity (Voytenko et al., 2015b). We also deployed TRI at Jakobshavn Glacier in June 2015. That deployment was also fortunate to capture calving, and here we draw a similar conclusion to that work, explicitly, that calving may be a multiday process made up of discrete, punctuated events (Xie et al., 2016).

Satellite-based interferometric synthetic aperture radar (InSAR) has been available for several decades (Rodriguez and Martin, 1992; Goldstein et al., 1993; Rignot, 1998; Joughin et al., 1999). However, a ground-based interferometric radar approach such as TRI offers significant advantages over both satellite observations and ground-based GPS in terms of spatial and temporal resolution. TRI generates displacement, velocity, and elevation updates every few minutes over wide swaths that can extend ~10 km in any direction. TRI avoids the temporal aliasing of time-varying processes inherent in satellite-based observations (where samples are typically collected every few days), while delivering spatial observations that are orders of magnitude better than sparse GPS networks. While TRI's interferometric observations of displacement and velocity are inherently scalar (it measures only the component of motion in the radar's line-of-sight direction), feature tracking can be employed to obtain two-dimensional velocity vectors with updates of several hours or less, depending on glacier speed (Peters et al., 2015; Xie et al., 2016).

The commercial TRI instrument that we used is a GAMMA interferometric, Ku-band (1.74 cm wavelength), real-aperture radar that provides high-resolution intensity and phase images. Operating at 17.2 GHz, instrument displacement sensitivity is better than 1 mm (Werner et al., 2008). The instrument has a nominal range resolution of 0.75 m, and an azimuth resolution of 7.5 m at a distance of 1 km, which decreases linearly with distance. The radar has one transmitting antenna and two receiving antennas, typically separated by a 25 cm baseline, positioned on a rotating frame (Figure 4a). The radar takes approximately two minutes to scan data from a 150° arc. Consecutive interferograms in

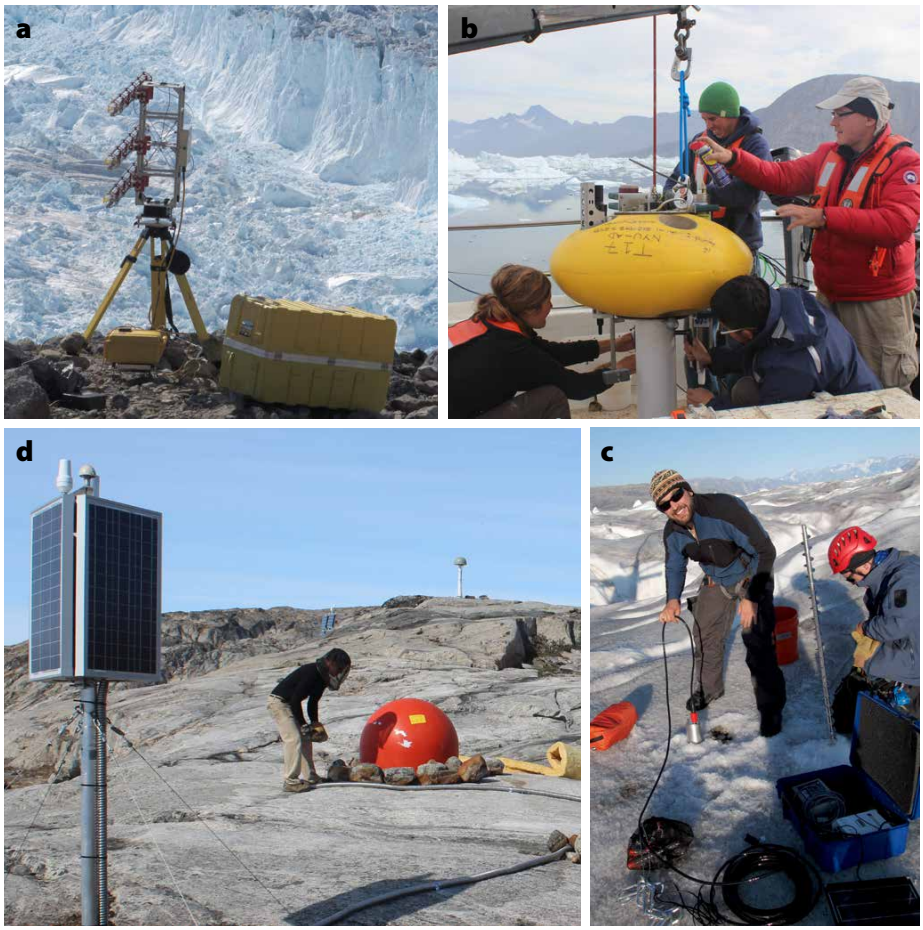

FIGURE 4. Deployment of field instrumentation at Helheim Glacier, August 2014. (a) TRI in the foreground with the ice mélange in the lower left and the calving front in the upper right background. (b) Tsunameter being prepared for deployment on the seafloor near Helheim Glacier. An array of five tsunameters was deployed. (c) On-glacier seismic and GPS deployment. An array of six collocated seismic-GPS devices were deployed along a flow line of the glacier. (d) Broadband seismometer deployed on land near the calving front. An array of two were deployed on opposite sides of the fjord near the calving front. An AWS with time-lapse camera was also installed (see article title page photo) adjacent to one of the seismometers.

time from one transmitting-receiving antenna pair are used to define the velocity. The two receiving antennas provide some redundancy, and if both are operating, they allow repeat mapping of glacier elevation to a vertical precision of about 3 m at 2 km distance (Strozzi et al., 2012). We use the ISP/DIFF/LAT (2016) software package to process the raw data into finished products. The combination of displacement, velocity, velocity change, elevation, and elevation change via rapid updates provides a powerful tool for calving studies.

Long-term TRI deployments have not yet found widespread use in glaciology, perhaps due to the instrument's cost, relative fragility, and power requirements, which can be challenging in the polar environment. We are working to remedy this situation, and in summer 2016 obtained one month of continuous, unattended TRI observations at Helheim. Eventually, we hope to observe calving at Helheim Glacier through its entire annual cycle.

To provide the reader with a sense of the kind of data product that TRI can produce, Figure S1 in the online supplemental materials shows a typical velocity field for Helheim from our TRI data using feature tracking and overlaying a coincident elevation field. The flow of the glacier in this instance is clearly plug-like, with shearing isolated to relatively thin basal and lateral boundary layers, so that the most important strain rate is longitudinal. In future deployments, we hope to deploy two radars in order to acquire rapid interferometric updates to the velocity field in stereo. This will be useful, as a single radar can only provide one component of velocity, while two can provide both components in the horizontal plane.

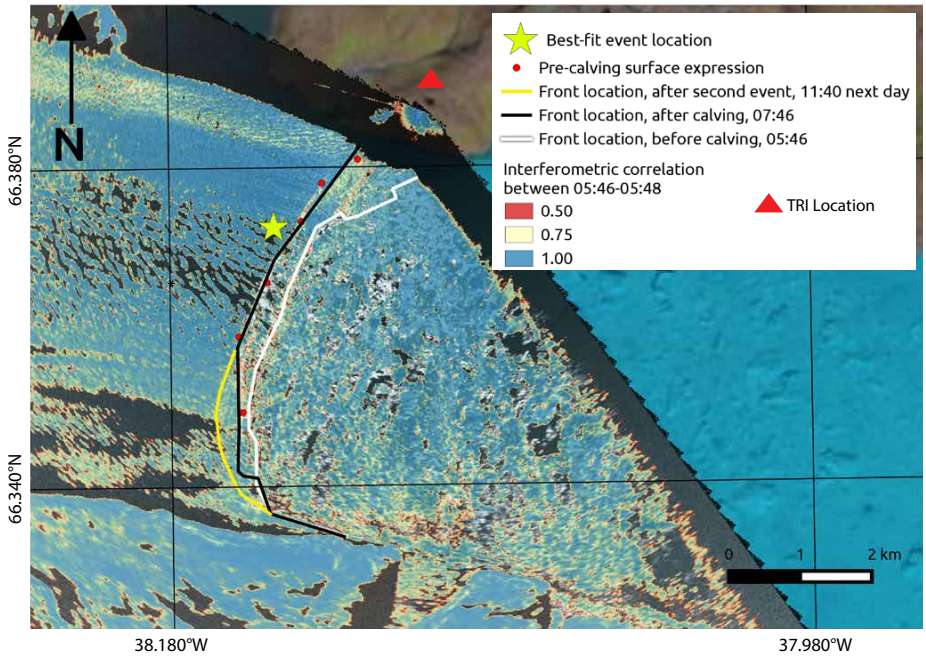

FIGURE 5. A map of interferometric correlation on August 12, 2014, during 05:46 and 05:48 UTC overlain on a Landsat 8 image of July 4, 2014 (one month prior to our fieldwork). High correlation values are shown in blue (indicating slow glacier motion) and low correlation values are shown in yellow and red (indicating fast motion). The TRI was positioned at the spot marked by the red triangle. The locations of the calving fronts before and after calving events are determined from individual TRI intensity images. The white line is the pre-calving terminus, the black line the primary calving event front, and the yellow line the secondary calving event. The formation of a low-correlation, crack-like, surface expression (denoted by red dots) at approximately 400 m upglacier of the pre-calving terminus is apparent. Precursory activity was detected along this line approximately one hour prior to the primary calving event. Most of this surface expression becomes the new terminus after the primary calving event (black line). A smaller secondary calving event took place a day later, affecting only the southern trunk (yellow line). The yellow star indicates the location of the main seismic event.

TRI Calving Detection

Although TRI has been typically used to determine relatively slowly evolving surface characteristics of glaciers such as tidal response (e.g., Voytenko et al., 2015b), TRI data can also be used to examine surface areas where rapid changes are taking place (e.g., Xie et al., 2016). Line-of-sight displacements of individual pixels near the calving front during the August 2014 TRI deployment (Figure S2) reveal a decrease in glacier velocity coincident with the primary calving event at 06:37 UTC on August 12. A secondary calving event only affected a portion of the southern trunk approximately one day later, at 11:31 UTC on August 13. Putting together the observations for the entire TRI scan area before, during, and after the primary calving event (Figure 5) reveals some of the complexity of the calving process. The initial glacier front peeled back in a multistep process. From radar intensity images, we can evaluate the position of the calving front and observe its multi-step retreat (Figure S3).

A useful metric for surface change can be derived from interferometric correlation, which measures the similarity of scattering characteristics between consecutive radar images (a high correlation implies that the surface is not changing). This metric is typically used to judge phase quality for interferometric phase unwrapping. Here, we use maps of interferometric correlation coefficients between successive two-minute images to determine periods of rapid surface change related to calving. Although the primary event took place at 06:37 UTC on August 12, we observed a strong drop in correlation around 05:46 UTC (approximately an hour before the primary calving event) along a linear, crack-like, surface expression about 400 m upstream of the terminus (Figure 5, red dots, and Figure S4). The location of this failure surface also marks the post-calving terminus position. These observations do not necessarily document the true start of the calving process, which may begin days in advance

of the primary calving event (James et al., 2014; Xie et al., 2016). Instead, the precursor event suggests the onset of rapid change in the glacier surface.

We evaluated the strain rate field over the northern trunk of the glacier by spatial differencing (in the horizontal direction) TRI velocity maps, adjusted to match the approximate direction of flow (Figure S5 and Voytenko et al., 2015a). The velocity maps were taken from 12 hours before the primary event, around the time of the main event, and 12 hours after to match the tidal phase. Close to the northern trunk, 12 hours before and shortly before calving, the ice front exhibited increased strain rates (extension), while the mélange was consistently under compression. We are unable to deduce from this if the glacier reached a critical strain rate, but it is likely that changes in strain rate occur well prior to calving.

TRI can produce rapid-update digital elevation maps (DEM) of Helheim Glacier. DEM accuracy is estimated to be approximately 3 m, and while not suitable for discerning subtler vertical motions of the glacier, it can certainly detect larger features, such as calving. From an evaluation of the ice front height prior to calving with that after calving (Figure 6 and Figure S6), we observe that prior to calving, the cliff reached approximately 100 m in height, and then failed. This observation is roughly in accord with the theoretical failure criteria provided by Bassis and Walker (2011).

From these TRI observations, we henceforth argue calving to be a process, spanning several days, stitched together by singular events, such as noted above, rather than a singular, short minute-scale event.

GPS

GPS devices measure ground motion in three dimensions, at higher frequency (period <1 min) and in greater precision (centimeter-level) than TRI. Moreover, TRI usually only provides a single component of motion (the projection of the true velocity vector onto the look vector of the TRI), whereas GPS data determine displacement in three dimensions. A shortcoming, however, is that GPS receivers can in general only be deployed at a handful of locations, and thus yield spatially sparse observations, while TRI provides effectively millions of measurements every few minutes.

To monitor higher-frequency (period <1 min) glacier motion, we installed six GPS stations (Figure 4c) along a central flowline on the northern trunk of the glacier. All GPS sites were deployed early on August 9, 2014, and retrieved later on August 15, 2014. One GPS site ceased recording a few hours after deployment due to an internal fault and a second site failed on the morning of August 11, 2014, after the anchor system melted out of the ice. Each site consisted of a dual-frequency receiver (Trimble NetRS 5700 with Trimble Zephyr Geodetic antennas) that collected moderate-rate (1 Hz) GPS data. Positions were determined using differential carrier phase positioning (Chen, 1998) relative to a permanent, fixed GPS receiver at the nearby town of

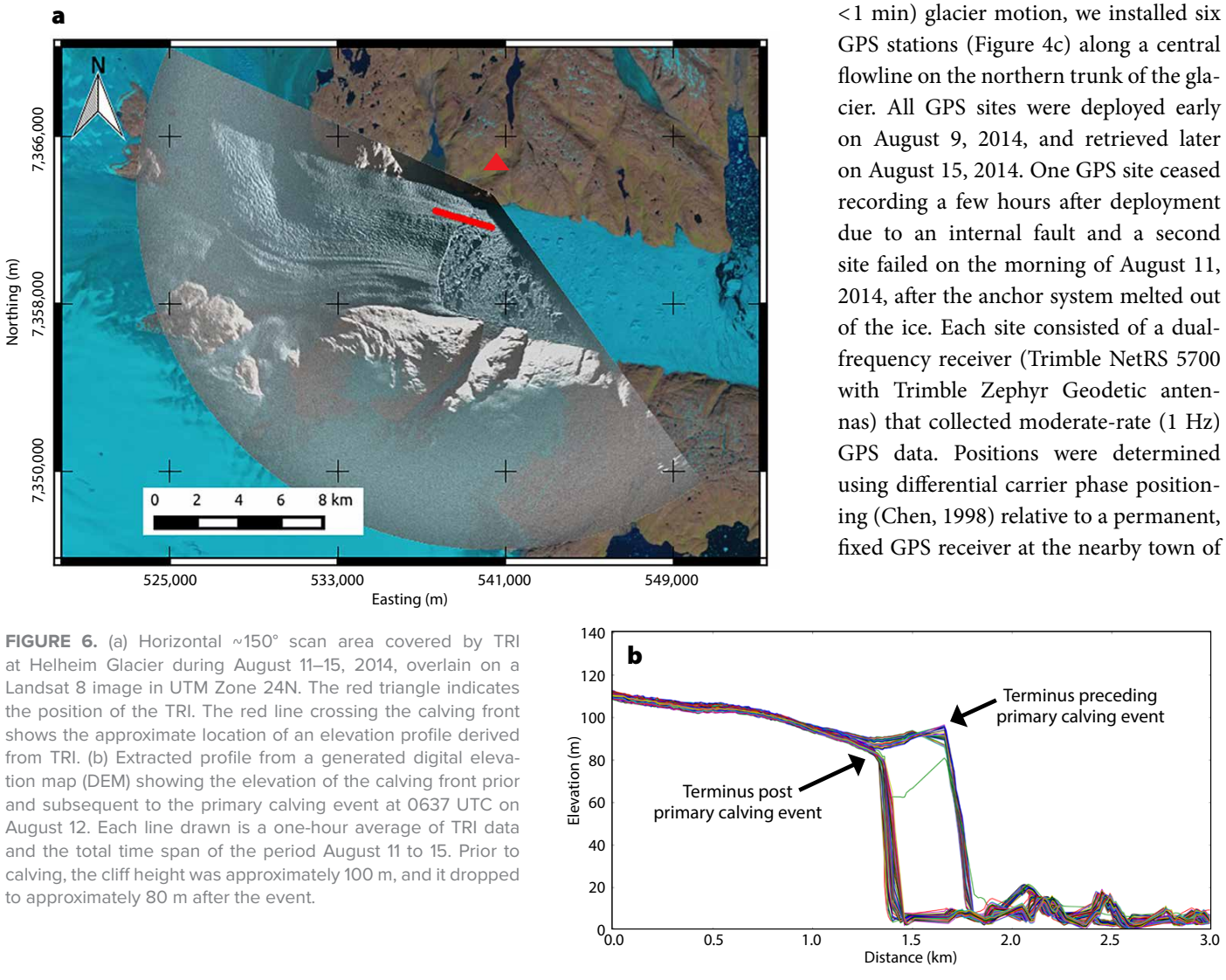

FIGURE 6. (a) Horizontal ~150° scan area covered by TRI at Helheim Glacier during August 11–15, 2014, overlain on a Landsat 8 image in UTM Zone 24N. The red triangle indicates the position of the TRI. The red line crossing the calving front shows the approximate location of an elevation profile derived from TRI. (b) Extracted profile from a generated digital elevation map (DEM) showing the elevation of the calving front prior and subsequent to the primary calving event at 0637 UTC on August 12. Each line drawn is a one-hour average of TRI data and the total time span of the period August 11 to 15. Prior to calving, the cliff height was approximately 100 m, and it dropped to approximately 80 m after the event.

Kulusuk (~100 km away). Horizontal and vertical uncertainties are approximately 5 cm and 10 cm, respectively. Geodetic solutions were transformed to a Northern Hemisphere polar stereographic projection centered on Greenland (origin at 90°N, 45°W; standard parallel of 70°N; referenced to the WGS84 ellipsoid; EPSG 3413) for distance and speed calculations.

GPS-derived glacier speeds vary from ~12.5 m d^{-1} to ~18.5 m d^{-1} (Figure 7). The site nearest the calving front has the highest speed, at ~18.5 m d^{-1} with variations of ~1 m d^{-1}. The upstream sites record motion of roughly the same speed (~12.5 m d^{-1} to 14 m d^{-1}) and character despite being separated by several kilometers, being installed in areas of differing surface slopes, and being subject to differing amounts of surface melt. All GPS sites exhibit diurnal fluctuations in speed. The timing of the daily speed peak (just prior to midnight UTC) and its undamped character at the upstream sites suggest that this daily speed peak may be the result of surface meltwater enhancing basal lubrication, and thus increasing sliding, as has been observed elsewhere on the Greenland Ice Sheet (Shepherd et al., 2009). The site nearest the calving front also exhibits a subtler, secondary peak (at ~1200 UTC, just before local low tide) that is not observed at the upstream sites, which could be related to tidal forcing, also inferred from TRI data (Voytenko et al., 2015b).

Glacier motion (speed and character) at the GPS sites remained unchanged after the primary calving event. Following the secondary calving event, however, speed increased at all GPS sites by ~1 m d^{-1} at the near-calving front site and ~0.5 m d^{-1} at the upstream sites. Speed peaked approximately one day after the secondary calving event, and speeds returned to their pre-calving values by ~1200 UTC on August 15, 2014. The low-frequency (daily or longer) character of the post-calving speed peak appears to be roughly symmetrical. The higher-frequency speed fluctuations are temporarily interrupted at the upstream sites, becoming similar to that near the calving front, which suggests that the glacier may temporarily partially decouple from the bed following the calving event, or that stresses are more efficiently transferred upstream for an approximately two-day period following calving.

Our GPS data suggest that the upstream effects of calving are limited until a full-width failure occurs of both the northern and southern trunks, indicating that even a relatively small portion of the glacier, in this case the southernmost trunk (~1.5 km wide), can provide significant backstress. This backstress might be redistributed to the remaining intact portion of the glacier following the larger, primary calving event. The post-calving glacier motion perturbation is also temporary, as glacier speed appears to return to its pre-calving values and character within two days of the termination of the calving process.

Passive Seismology

Seismometers can provide ground velocity in three components by measuring accelerations. We used broadband instruments that cover a wide range of frequencies (well below 1 Hz), thus allowing observation of glacier and land velocity at a much higher rate than is provided by our GPS or TRI instruments. The benefit of installing seismometers on the glacier is that they are sensitive to icequake (high frequency cracking of the glacier) and sudden slip events (short duration increases well above background speeds). The advantage of installing them on nearby land is that the stations can be utilized for a much longer period of time (several years). We established on-land sites on a rolling basis over the last several years (Figure 4d) with one

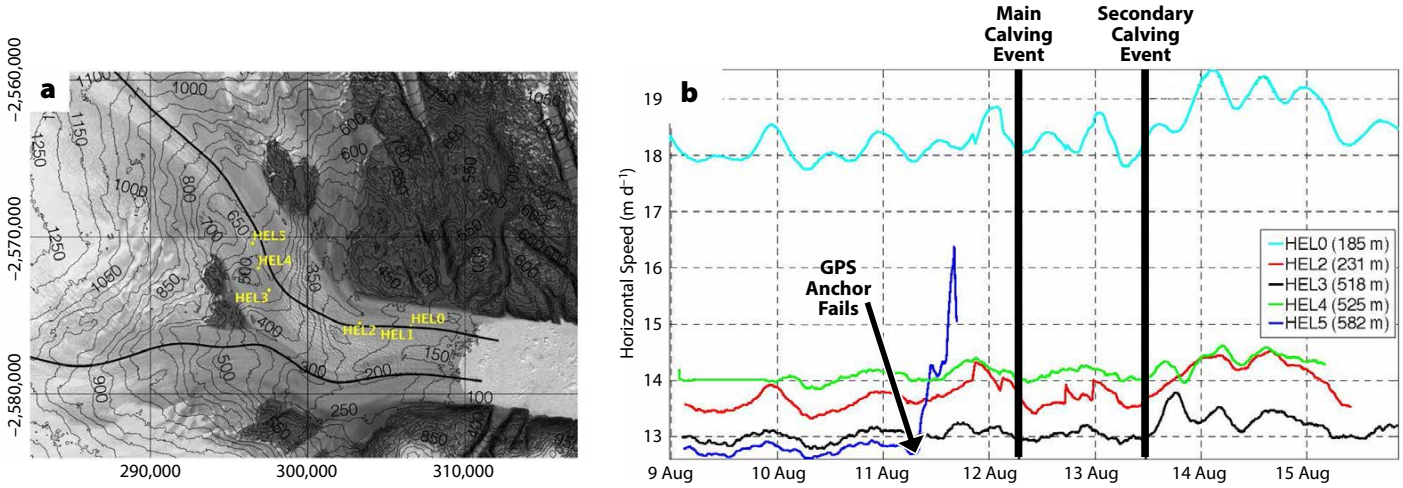

FIGURE 7. Glacier horizontal speed derived from GPS measurements. (a) Location map showing the positions of the GPS sites (the on-glacier seismometers were collocated with the GPS). The background is a panchromatic Landsat 8 image acquired July 4, 2014. Contours (50 m interval) indicate elevation relative to WGS84 ellipsoid (Howat et al., 2014). The coordinate system (m) is a Northern Hemisphere polar stereographic projection centered on Greenland (origin at 90°N, 45°W; standard parallel of 70°N; referenced to the WGS84 ellipsoid; EPSG 3413). (b) Glacier horizontal speed derived from GPS measurements. Elevations of GPS sites are noted in the legend. The time of primary and secondary calving events are marked (black, vertical solid line). The anchor on the furthest upstream device failed on August 11, 2016, and the station slid several meters downhill before the power system failed, resulting in high apparent speeds that are not representative of glacier motion.

site in August 2012 (HEL1 – Nanometrics Trillium 120), another in August 2013 (HEL2 – Nanometrics Trillium 240), and two others in August 2014 (HEL3 and HEL4 – Nanometrics Trillium 240). These broadband seismometers continue to operate. On the glacier, we established a seismic array (Nanometrics Trillium Compact Posthole) in the vicinity of the Helheim calving front, along a flow line on the glacier (Figure 4c) collocated with the GPS array mentioned above. In addition, on land, we installed Nanometrics Trillium 120s on opposite sides of the calving front (Figure 4d).

When a calving event happens, the seismic waves that emanate from the glacial fracture take different amounts of time to reach each seismic station, depending on the distance from the fracture to the station. It is then a straightforward calculation to invert for location, given a standard velocity of seismic waves through ice and travel time to each station. Surprisingly, we found that the calving energy propagated at a much slower speed (~1,600 m s^{-1}) than the typical compressional wave speed in ice (3,800 m s^{-1}). We developed a method of determining glacier calving locations using seismic wave arrival times from paired local seismic stations (Mei et al., 2016). In short, the difference in surface wave arrival times for each pair of stations is used to define a locus (hyperbola) of possible origins. With multiple pairs, this can be used to triangulate the origin of the seismic waves, interpreted as the calving location. Our different approach was motivated by difficulties with traditional seismic location methods that fail due to the emergent nature of calving, which obscures the primary and secondary wave onsets, and the close proximity of the seismometers, which combines body and surface waves into one arrival. As a summary of that previous work, locations determined from seismic data match the location of calving determined by time-lapse cameras and remote sensing.

On August 12, while camped near the calving front, our team was awoken by a sustained, loud rumbling noise. Three of the seismometers recorded vibrations that occurred during the primary calving event at this moment (Figure 8). One of the stations was deployed on the glacier surface, while the other two were well above the glacier, on nearby land. From the seismic data collected, we were able to ascertain that the peak of the calving event, the primary in a seismic sense, occurred at 06:37 UTC. Using cross-correlation of the seismic signals, we determined the difference in arrival times, and from this, estimated the calving location. In fact, two different methods are used to estimate the calving event location, and they produce similar results, indicating the same location on the northern glacier trunk. In the first method, travel times from all three seismic stations are used simultaneously to find the most likely singular point of origin of the calving signal, which is shown as the blue X in Figure 9. In the second method, seismic stations are used in only a pairwise sense and this results, instead of a point location, in an area as shown by the blue triangle in Figure 9 (details in Mei et al., 2016).

From a TRI map of interferometric correlation (Figure 5), we reported a precursor event nearly an hour prior to the primary calving. The formation of this TRI surface expression seems to be related to seismic activity around the same time (Figure S7). Evidence of precursory activity, from both TRI and seismic data, gives us greater confidence in asserting that calving is a process made up of a number of punctuated events. Calving of large ice masses may be a similar process to earthquakes in that earthquake foreshocks sometimes culminate in much larger earthquakes. We note that there are also several periods of high glaciogenic seismic energy visible on seismograms that do not culminate in a large calving event. Detailed analysis of the high-frequency on-ice seismicity is the subject of ongoing study.

Parenthetically, the bedrock elevation of Helheim Glacier indicates that the bedrock is deeper beneath the northern half of the trunk (Figure 9), a fact that may be linked to where the glacier preferentially calves, suggesting that a glacier grounded on deeper bedrock, or the deeper portions of a calving front, may be more susceptible to calving.

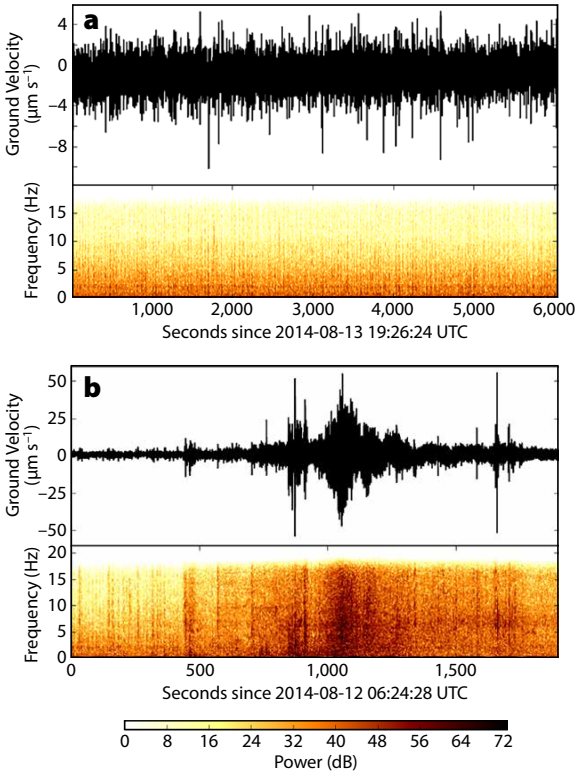

FIGURE 8. Time and frequency analysis of seismic signals. (a) The upper subpanel shows a time series of noise recorded by a Helheim on-land seismometer during a non-calving period. The vertical axis denotes seismic ground velocity, which is typically of order 1 μm s^{-1}. The lower subpanel is a time series of seismic activity energy presented as a spectrogram. The vertical axis is frequency in Hz, showing that the bulk of the noise energy is found below 1 Hz. (b) The upper subpanel shows a time series of an August 12, 2014, calving event, during which the seismic ground velocity reached 50 μm s^{-1}, more than an order of magnitude higher than the ambient noise seen in panel (a). The lower subpanel shows that the calving event also presents much higher frequency intensities. By eye, one can see that the calving event provides energy in the 2 Hz to 18 Hz frequency range, clearly distinguishing it from the background noise.

Tsunameters

Another way to track glacier activity is to monitor nearby ocean waves. These waves can be excited by changes at the glacier front that propagate into the ocean, or vice versa, and thus have the potential to provide complementary information about the calving process.

An array of seafloor moorings was deployed in Sermilik Fjord prior to our field campaign. Tsunameters installed on each mooring were used to detect calving events in the fjord. The tsunameters sampled every four seconds, which allowed for detection of the fast barotropic waves traveling along the fjord. At the time of the primary August 12, 2014, event, two tsunameters were active (see Figure 10a for their locations). The one closer to the calving front was located about 70 km away at depth of 880 m, and the farther one was 84 km away at depth of 908 m.

A propagating barotropic wave associated with each calving event was detected on both active tsunameters (Figure 10b). The signal of the primary calving event reached the closest sensor between 6:51 and 6:53 UTC with amplitude of 10 cm. Approximately 160 seconds later, the signal arrived at the farther one. Using a mean propagation speed of calving waves in Sermilik Fjord, a barotropic signal generated at the calving front location takes between 14.7 and 17.1 minutes to reach the closer sensor. This rough calculation suggests the first calving event was initiated sometime between 6:34 and 6:39 UTC.

The smaller secondary event reached only one quarter of the amplitude of the primary event and arrived at the closer tsunameter around 11:40 UTC, at the farther one again with 160 second lag. The tsunameter data thus estimate the second event was initiated between 11:31 and 11:36 UTC, August 13.

The spectral and propagation characteristics of these waves are consistent with those of other calving-generated waves observed in Sermilik Fjord (Vaňková and Holland, 2016). In the cited study, a numerical model suggested that the effect of calving on the ocean is equivalent to a damped oscillator boundary forcing with oscillation period between 5 and 10 minutes and damping time scale of 10 minutes. We conclude from our ocean-based observations that in the instance of the calving events we observed in August 2014, calving created a wave response in the ocean, and not vice versa. We also note that going forward, seafloor tsunameter arrays are an effective way to monitor calving of an outlet glacier. Such arrays can be placed at significant distance from the calving front, for example, tens of kilometers, thus safely away from the calving front and the mélange. Broadband seismic stations at coastal locations may also be capable of providing similar information (Amundson et al., 2012).

AWS

A cursory analysis of our AWS data (air temperature, radiation, wind, and precipitation) did not reveal any obvious link to the observed calving events during our week-long observation period, which is perhaps not surprising. From our AWS time-lapse cameras (Figure 11), we know the precise position of the calving front before and after the various calving events. It is reassuring to find that the locus of the calving energy as determined from the seismic data (Figure 9) is located near the calving front, as revealed by the camera images.

The northern and southern trunks of Helheim Glacier meet along a medial moraine, evident in Figure 11 as a dark line consisting of rock and dust following along a flow line. This suture zone, where two glacier streams meet, likely has a different structural makeup than the ice elsewhere in either trunk, and we speculate that it plays a role in the nature of the calving we witnessed (i.e., the secondary event occurred only over the southern trunk; Walker et al., 2015).

Anecdotally, while flying over the glacier several days before the calving events, we noticed a significant amount of water collected in surface crevasses. Several days after the calving events, we again flew over the glacier and noted that most of the surface water had disappeared. Our AWS cameras were not adequately positioned to show the surface water, and thus we are unable to say when the water drained and if it had any possible relation

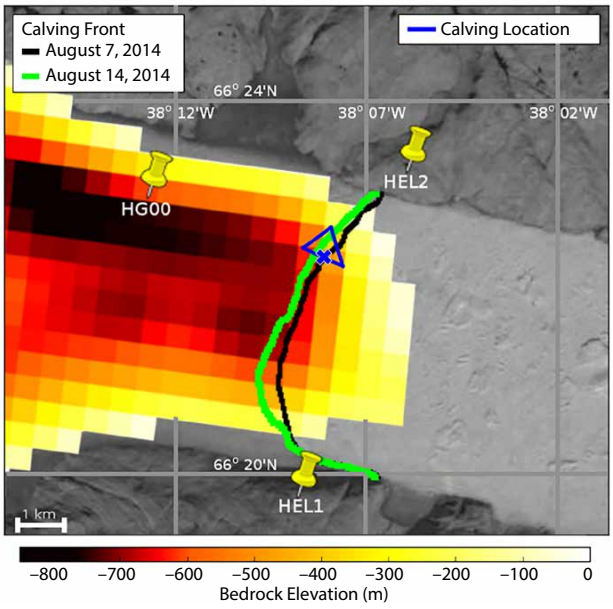

FIGURE 9. Plan view illustration of calving event detection and location using a seismic array. Stations marked HEL1 and HEL2 are situated on the rock sidewalls of the glacial fjord at an elevation of approximately 400 m, while station HG00 is located on the glacier trunk at an elevation of approximately 100 m. The background image is from Landsat 8 on August 7, 2014. The light gray background grid indicates latitude and longitude. Overlain in center left is a shaded plot of the bedrock elevation (Leuschen and Allen, 2013) beneath the grounded glacier trunk but not below the mélange. The black line indicates the pre-calving terminus while the green line shows the terminus after the primary calving event, both estimated from camera images taken at the AWS. Helheim Glacier is to the west (left) of the calving front, and the mélange is to the east (right). The blue triangle and the blue X symbol indicate the location of calving onset as determined from seismic triangulation.

to the calving events.

The AWS camera was in operation prior to our field campaign, and time-lapse images made over the preceding year show the aperiodic nature of the calving events at Helheim (Figure S8). It is evident from year-long time-lapse cameras that Helheim Glacier generally advances in winter and retreats in summer, highlighting the fact that there is an atmospheric influence on calving. The mechanism by which the atmosphere impacts seasonal calving remains unclear, requiring further observational data.

TOWARD PARAMETERIZED CALVING

As mentioned earlier, our overarching goal is to develop a parameterization of calving. A practical first step toward this goal is to build a detailed process model using theory motivated by observations that can accurately simulate aspects of the calving process (Figures 5 and 6). Such a process model is likely not suitable for use in a large-scale, long-simulation climate model, but can serve to guide the construction of a simplified parameterization of calving to be used in a climate model. This parameterization goal is well beyond the scope of the present work, in which we are only reporting on one observation of calving, and our first steps toward detailed modeling of the phenomenon.

Glacier flow can only be accurately modeled provided one knows the rheology of the ice (i.e., the relation between the strain rate and the stress fields). The viscous rheology appropriate to a slowly flowing glacier undergoing creep is relatively well known (Glen, 1958), as is the elastic rheology appropriate to bending (Timoshenko and Goodier, 1970). The plastic rheology that is perhaps appropriate to a fast-moving glacier that is fracturing and calving, such as Helheim Glacier, is unknown. Current generation glacier models do not simulate calving in a realistic manner, but progress is being made by considering damage mechanics (e.g., Krug et al., 2014). While such models do describe the viscous and elastic behavior of glaciers based on an assumed relation between strain (or strain rate) and stress, they do not yet describe the failure associated with plastic flow, which is independent of strain and strain rate, complicating matters greatly. Future modeling advancements, based on observations reported here and elsewhere, should improve our ability to model the plastic failure stress that glaciers such as Helheim likely undergo. Specifically, our future observational efforts at Helheim will be targeted at providing the data necessary to modify the glacier rheology to include a plastic yield curve. This will be carried out following the analogous theoretical framework that is widely used in the sea ice literature and is successful in modeling sea ice plastic failure (Hibler, 1979).

Based on an existing two-dimensional, along-flow line model (Parizek et al., 2013), we have begun to model the stress state of Helheim Glacier. As a starting point, we are simulating the viscous and elastic stress fields. When and where a glacier such as Helheim ultimately fails depends not only on its material strength and the many imperfections that limit it, but also on the crack-forming viscous (Figure 12) and elastic (Figure S9) differential stress fields to which it is subjected as it completes its journey to the ocean. Within a field of crevasses, theory indicates ~320 kPa of tensile stress is necessary to generate new crevasses, with that threshold decreasing to ~30–80 kPa for individual crevasses (van der Veen, 1998). For a calving event to take place, surface and/or basal crevasses must penetrate the full glacier thickness. In the viscous realm, crevassing often takes place along lateral shear margins, where there are transitions in basal topography and/or drag, and proximal to the ice front, where differences between the glaciostatic and hydrostatic pressures across the interface lead to enhanced deviatoric stresses within the ice that maintain the overall force balance. The glacier surface steepens just downstream of regions with topographic highs and/or enhanced basal drag to drive flow across these features, with the resulting changes in flow

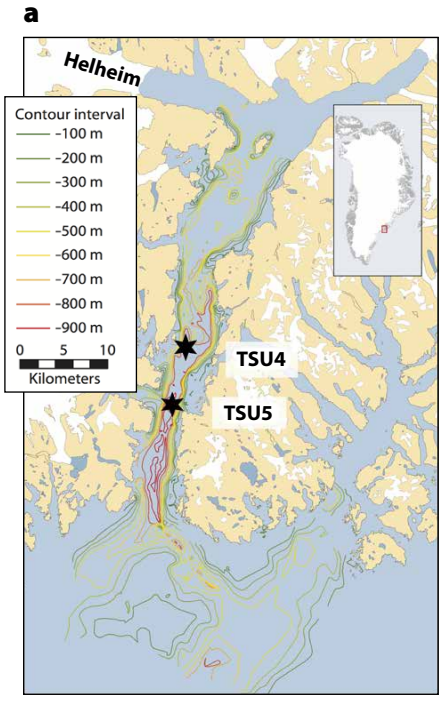

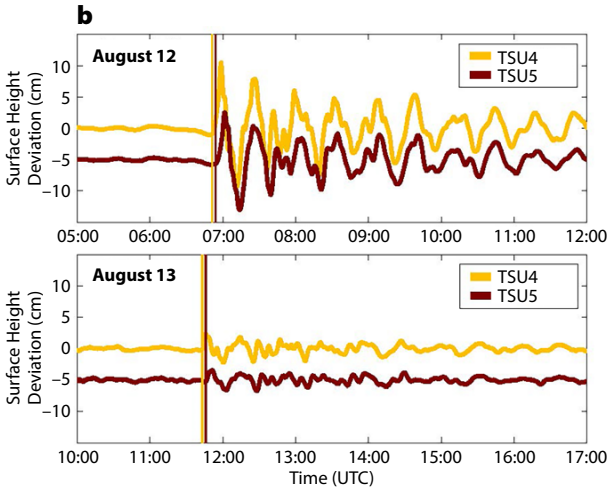

FIGURE 10. Location of the ocean tsunameter array and the detection of calving events. (a) Helheim Glacier and Sermilik Fjord with bathymetric contours and mooring locations marked with black stars (reprinted with permission from Schjøth et al., 2012). (b) Tsunami waves caused by the two calving events and detected on pressure sensors. Vertical lines indicate the onset of the calving signal on each tsunameter. TSU5 is offset by 5 cm for clarity.

speed leading to tensional longitudinal stresses within the glacier. Furthermore, tensional stresses also develop across an onset region of an ice shelf or ice tongue as basal traction vanishes where the base of the glacier loses contact with the solid Earth. Finally, within a few thicknesses or less of a marine-terminating glacier front, the stress state within a glacier also favors failure due to the glaciostatic/hydrostatic pressure imbalance between the glacier front and the combination of air and seawater into which it is flowing (Figure 12), as well as the tidal flexure of the floating tongue (Figure S9). At this stage, it is not yet clear from observation if any, some, or all of these detailed factors need be included in a parameterization of calving.

While our modeling effort is currently aimed at a deterministic simulation of calving, as is appropriate in the context of developing a process-oriented understanding of calving, it may turn out that such a deterministic approach is not feasible in the context of large-scale, long-simulation climate modeling. An alternative approach for a calving parameterization has been to invoke a probability distribution, with calving considered a random event drawn from an underlying distribution (Bassis, 2011). The empirical relationships or probability distributions appear to depend strongly on the characteristics of a specific outlet glacier (e.g., bed slope, the presence of an ice shelf, thickness above flotation). While we here present observations of just one calving event and seek in the future to collect many more, there may be merit in the ultimate parameterization of calving as a random event. Clearly, a large database of calving events is required in order to build a viable probability distribution to give this approach a significant foundation. This is also one of our long-term goals.

While calving has obvious relevance to glaciology, it is also germane to oceanography, albeit indirectly. This is particularly so in the context of freshwater release arising from melting of Greenland's icebergs into the North Atlantic Ocean and its impact on ocean stratification, and thus on open-ocean convection and deepwater formation (Weijer et al., 2012; Böning et al., 2016). It is important to understand where large icebergs go and where they melt, but it is important as a starting point to know where icebergs are produced and what is their size distribution. The type of calving parameterization we seek here through our glaciological modeling efforts feeds directly into this principal need in oceanographic modeling.

SUMMARY

Using a suite of instrumentation, we sought to collect data that would help us gain insight into key questions relating to calving. Here, we reiterate these questions, and summarize our responses.

How does the strain (rate) field evolve during calving?

Through TRI measurements, we observed variability in the horizontal strain rate 12 hours before, during, and 12 hours after the primary calving event. The calving detected August 12–13, 2014, consisted of precursor, primary, and secondary events. Well prior to calving, the glacier strained in a fashion that showed larger strain rates near the calving front, lesser rates upstream, and lesser rates after the calving. The first strong indication of calving occurred approximately one hour prior to the primary calving event (based on interferometric correlation measurements), with rapid changes in the surface observed along a transverse front that was destined to become the new terminus.

Does calving lead to acceleration of the glacier?

From GPS near the glacier front, along a flowline of the northern trunk, a significant increase in speed was detected only following the secondary calving event, and not following the primary event. Similar behavior was seen in the TRI. This post-calving increase in speed vanished after an additional two days, as the glacier readjusted to its pre-calving motion.

FIGURE 11. Photographs from the AWS time-lapse camera situated on the south side of Helheim Fjord. The left panel shows the calving front demarcated by an orange line on August 12, 2014, at 06:00 UTC, prior to calving. The glacier is flowing left to right and is approximately 6 km wide. To the left of the calving front, a dark along-flow line is a medial moraine that separates the narrower, shallower southern trunk of the glacier from the wider, deeper northern trunk. The mélange is to the right of the calving front. The right panel shows the front at 07:00 UTC, after the primary calving event, with the orange line from the top panel overlain for reference.

Is there a relation between calving and cliff height?

Fairly consistent with existing theoretical estimates, we noted that the cliff height of the pre-calving ice front was approximately 100 m, and the post-calving height was 80 m. This lends some credence to the theoretical construct that only a certain height of cliff can be mechanically supported by intrinsic glacier strength.

Or between calving and water depth?

We detected calving that occurred first along the deeper northern trunk of the glacier, and second along the shallower southern trunk. This offers some backing to the theoretical concept that glaciers in deeper water are more likely to calve than those in shallow water, again a mechanical support argument. It should also be pointed out that the combination of cliff height and water depth (i.e., closeness to flotation) may also play a role, but is not investigated here.

Can seismic signals from a close-array locate a calving event?

Using triangulation from combined on-glacier and on-land broadband seismometers, and corroborated by AWS cameras and TRI, we found that seismically determined calving location coincided with the post-calving terminus. Moreover, the seismic array pointed to a particular portion of the ice front as being the most active area, coinciding with the deepest bed at the front.

Does atmospheric variability play a role in calving?

Our AWS instruments did not record any atmospheric properties that would have a direct bearing on the witnessed calving events. As changes in upglacier surface meltwater ponding within crevasses were not observed, this does not rule out the impact of atmospheric variability on glacier calving, particularly on the longer seasonal time scale.

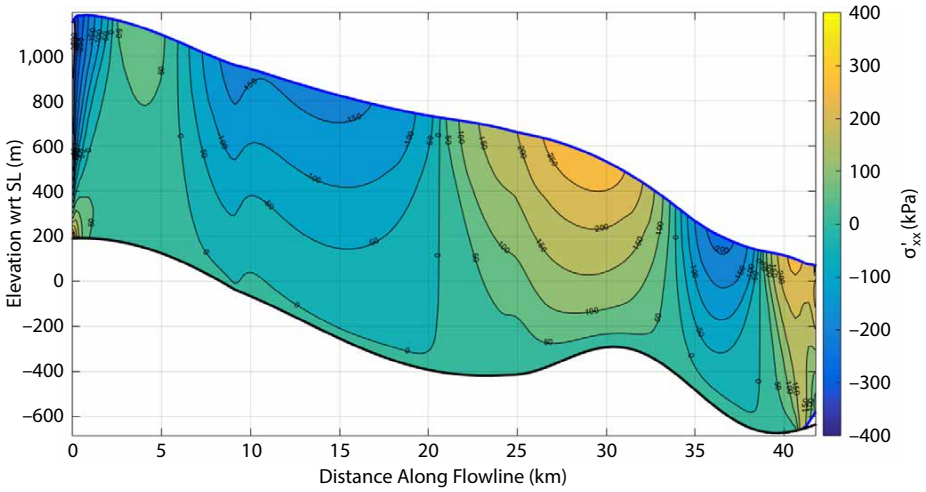

FIGURE 12. Simulation of viscous stresses in a two-dimensional (vertical slice) along-flow-line glacier model (glacier flow is from left to right). The stresses are generated by the glacier flowing over irregular bed geometry (bumps and depressions). The longitudinal deviatoric stress field is shown as color shading (positive for tension and negative for compression). The glacier front is located at approximately position 41.5 km, at the far right.

Do ocean waves trigger calving?

For the discrete calving events we observed, it is unequivocal that the glacier calving preceded an ocean tsunami response. This suggests that high-frequency ocean swell did not play a role in triggering calving, and in fact just the opposite. This does not rule out ocean tides (high/low or spring/neap) playing a part in this calving event as tides over a long time period may promote wear on the many fracture surfaces and ultimately promote weakening.

In summary, this pilot study has sought improved understanding of calving at Helheim Glacier, and Greenland tidewater glaciers in general. We have seen that among important observations needed to understand calving are the evolution of the height of the cliff at the glacier front, the depth of the ocean, and the strain rate near the calving front. There are also observations from inside or beneath the glacier, such as the occurrence of basal crevasses, that we do not yet have the capability to observe, but are likely important. Our observations reinforce the idea that calving is a cumulative process, made up of a number of discrete events that occur over a number of days. We again caution that our observations are from a single glacier and may not generalize to others. Whether or not the observed, cumulative nature of calving will play a role in the parameterization of calving remains a question for future study. The noted temporal span of the calving process may, for instance, have ramifications for the time stepping of model parametrization of the process. Continued development of numerical models, deterministic or probabilistic, with realistic glacier failure criteria built on rheology consistent with field observations, may ultimately lead to usable parameterizations that can make future sea level projections more robust.

SUPPLEMENTAL MATERIAL

Supplemental Figures S1–S9 are available online at https://doi.org/10.5670/oceanog.2016.98.

REFERENCES

Alley, R.B., H.J. Horgan, I. Joughin, K.M. Cuffey, T.K. Dupont, B.R. Parizek, S. Anandakrishnan, and J. Bassis. 2008. A simple law for ice-shelf calving. *Science* 322(5906):1,344, https://doi.org/10.1126/science.1162543.

Amundson, J.M., J.F. Clinton, M. Fahnestock, M. Truffer, M.P. Lüthi, and R.J. Motyka. 2012. Observing calving-generated ocean waves with coastal broadband seismometers, Jakobshavn Isbræ, Greenland. *Annals of Glaciology* 53(60):79–84, https://doi.org/10.3189/2012/AoG60A200.

Amundson, J.M., M. Fahnestock, M. Truffer, J. Brown, M.P. Luthi, and R.J. Motyka. 2010. Ice mélange dynamics and implications for terminus stability, Jakobshavn Isbræ, Greenland. *Journal of Geophysical Research* 115, F01005, https://doi.org/10.1029/2009JF001405.

Amundson, J.M., and M. Truffer. 2010. A unifying framework for iceberg-calving models. *Journal of Glaciology* 56(199):822–830, https://doi.org/10.3189/002214310794457173.

Amundson, J.M., M. Truffer, M.P. Lüthi, M. Fahnestock, M. West, and R.J. Motyka. 2008. Glacier, fjord, and seismic response to recent large calving events, Jakobshavn Isbræ, Greenland. *Geophysical Research Letters* 35, L22501, https://doi.org/10.1029/2008GL035281.

Bartholomaus, T.C., J.M. Amundson, J.I. Walter, S. O'Neel, M.E. West, and C.F. Larsen. 2015. Subglacial discharge at tidewater glaciers revealed by seismic tremor. *Geophysical Research Letters* 42(15):6,391–6,398, https://doi.org/10.1002/2015GL064590.

Bassis, J.N. 2011. The statistical physics of iceberg calving and the emergence of universal calving laws. *Journal of Glaciology* 57(201):3–16, https://doi.org/10.3189/002214311795306745.

Bassis, J.N., and C.C. Walker. 2011. Upper and lower limits on the stability of calving glaciers from the yield strength envelope of ice. *Proceedings of the Royal Society A*, https://doi.org/10.1098/rspa.2011.0422.

Benn, D.I., C.R. Warren, and R.H Mottram. 2007. Calving processes and the dynamics of calving glaciers. *Earth-Science Reviews* 82:143–179, https://doi.org/10.1016/j.earscirev.2007.02.002.

Böning, C.W., E. Behrens, A. Biastoch, K. Getzlaff, and J.L. Bamber. 2016. Emerging impact of Greenland meltwater on deepwater formation in the North Atlantic Ocean. *Nature Geoscience* 9:523–527, https://doi.org/10.1038/ngeo2740.

Bromirski, P.D., O.V. Sergienko, and D.R. MacAyeal. 2010. Transoceanic infragravity waves impacting Antarctic ice shelves. *Geophysical Research Letters* 37, L02502, https://doi.org/10.1029/2009GL041488.

Brown, C.S., M.F. Meier, and A. Post. 1982. *Calving Speed of Alaska Tidewater Glaciers with Applications to the Columbia Glacier, Alaska*. US Geological Survey Professional Paper 1258-C, 13 pp.

Caduff, R., F. Schlunegger, A. Kos, and A. Wiesmann. 2015. A review of terrestrial radar interferometry for measuring surface change in the geosciences. *Earth Surface Processes and Landforms* 40(2):208–228, https://doi.org/10.1002/esp.3656.

Chen, G. 1998. *GPS Kinematics Positioning for Airborne Laser Altimetry at Long Valley, California*. PhD thesis, Massachusetts Institute of Technology, Cambridge, MA, USA.

Colgan, W., H. Rajaram, W. Abdalati, C. McCutchan, R. Mottram, M. Moussavi, and S. Grigsby. 2016. Glacier crevasses: Observations, models and mass balance implications. *Reviews of Geophysics* 54:119–161, https://doi.org/10.1002/2015RG000504.

De Angelis, H., and P. Skvarca. 2003. Glacier surge after ice shelf collapse. *Science* 299(5612):1,560–1,562, https://doi.org/10.1126/science.1077987.

DeConto, R.M., and D. Pollard. 2016. Contribution of Antarctica to past and future sea-level rise. *Nature* 531(7596):591–597, https://doi.org/10.1038/nature17145.

Goldstein, R.M., H. Engelhardt, W.B. Kamb, and R.M. Frohlich. 1993. Satellite radar interferometry for monitoring ice sheet motion: Application to an Antarctic ice stream. *Science* 262:1,525–1,530, https://doi.org/10.1126/science.262.5139.1525.

Glen, J.W. 1958. The flow law of ice: A discussion of the assumptions made in glacier theory, their experimental foundations and consequences. *International Association of Hydrological Sciences Publishing* 47:171–183.

Hibler, W.D. 1979. A dynamic thermodynamic sea ice model. *Journal of Physical Oceanography* 9(4):815–846, https://doi.org/10.1175/1520-0485(1979)009<0815:ADTSIM>2.0.CO;2.

Holland, D.M., R.H. Thomas, B. DeYoung, M.H. Ribergaard, and B. Lyberth. 2008. Acceleration of Jakobshavn Isbræ triggered by warm subsurface ocean waters. *Nature Geoscience* 1:659–664, https://doi.org/10.1038/ngeo316.

Howat, I.M., I. Joughin, S. Tulaczyk, and S. Gogineni. 2005. Rapid retreat and acceleration of Helheim glacier, east Greenland. *Geophysical Research Letters* 32, L22502, https://doi.org/10.1029/2005GL024737.

Howat, I.M., A. Negrete, and B.E. Smith. 2014. The Greenland Ice Mapping Project (GIMP) land classification and surface elevation datasets. *The Cryosphere* 8:1,509–1,518, https://doi.org/10.5194/tc-8-1509-2014.

IPCC (Intergovernmental Panel on Climate Change). 2007. *Climate Change 2007: The Physical Science Basis. Contribution of Working Group I to the Fourth Assessment Report of the Intergovernmental Panel on Climate Change*. S. Solomon, D. Qin, M. Manning, Z. Chen, M. Marquis, K.B. Averyt, M. Tignor and H.L. Miller, eds, Cambridge University Press, Cambridge, United Kingdom, and New York, NY, USA, 996 pp.

IPCC. 2013. *Climate Change 2013: The Physical Science Basis. Contribution of Working Group I to the Fifth Assessment Report of the Intergovernmental Panel on Climate Change*. T.F. Stocker, D. Qin, G.-K. Plattner, M. Tignor, S.K. Allen, J. Boschung, A. Nauels, Y. Xia, V. Bex, and P.M. Midgley, eds, Cambridge University Press, Cambridge, United Kingdom, and New York, NY, USA, 1,535 pp.

ISP/DIFF/LAT. 2016. GAMMA Processing Software: Interferometric SAR Processor (ISP), Differential Interferometry and Geocoding package (DIFF), and Land Application Tools (LAT), http://www.gamma-rs.ch/no_cache/software.html.

James, T.D., T. Murray, N. Selmes, K. Scharrer, and M. O'Leary. 2014. Buoyant flexure and basal crevassing in dynamic mass loss at Helheim Glacier. *Nature Geoscience* 7(8):593–596, https://doi.org/10.1038/ngeo2204.

Joughin, I., W. Abdalati, and M. Fahnestock. 2004. Large fluctuations in speed on Greenland's Jakobshavn Isbrae glacier. *Nature* 432:608–610, https://doi.org/10.1038/nature03130.

Joughin, I., R.B. Alley, and D.M. Holland. 2012. Ice sheet response to oceanic forcing. *Science* 338(6111):1,172–1,176, https://doi.org/10.1126/science.1226481.

Joughin, I., L. Gray, R. Bindschadler, S. Price, D. Morse, C. Hulbe, K. Mattar, and C. Werner. 1999. Tributaries of West Antarctic ice streams revealed by RADARSAT interferometry. *Science* 286:283–286, https://doi.org/10.1126/science.286.5438.283.

Joughin, I., I.M. Howat, R.B. Alley, G. Ekstrom, M. Fahnestock, T. Moon, M. Nettles, M. Truffer, and V.C. Tsai. 2008. Ice-front variation and tidewater behavior on Helheim and Kangerdlugssuaq Glaciers, Greenland. *Journal of Geophysical Research* 113, F01004, https://doi.org/10.1029/2007JF000837.

Krug, J., J. Weiss, O. Gagliardini, and G. Durand. 2014. Combining damage and fracture mechanics to model calving. *The Cryosphere* 8(6):2,101–2,117, https://doi.org/10.5194/tc-8-2101-2014.

Leuschen, C., and C. Allen. 2013. IceBridge MCoRDS L3 Gridded Ice Thickness, Surface, and Bottom, Version 2, Helheim_2008_2012_Composite. NASA DAAC at the National Snow and Ice Data Center. Boulder, Colorado, http://nsidc.org/data/docs/daac/icebridge/irmcr3.

Levermann, A., T. Albrecht, R. Winkelmann, M.A. Martin, M. Haseloff, and I. Joughin. 2012. Kinematic first-order calving law implies potential for abrupt ice-shelf retreat. *The Cryosphere* 6(2):273–286, https://doi.org/10.5194/tc-6-273-2012.

Luckman, A., T. Murray, R. de Lange, and E. Hanna. 2006. Rapid and synchronous ice-dynamic changes in East Greenland. *Geophysical Research Letters* 33, L03503, https://doi.org/10.1029/2005GL025428.

MacAyeal, D.R., E.A. Okal, R.C. Aster, and J.N. Bassis. 2009. Seismic observations of glaciogenic waves (micro-tsunamis) on icebergs and ice shelves. *Journal of Glaciology* 55(190):193–206, https://doi.org/10.3189/002214309788608679.

Mei, M.J., D.M. Holland, S. Anandakrishnan, and T. Zheng. 2016. A two-station seismic method to localize glacier calving. *The Cryosphere Discussion*, https://doi.org/10.5194/tc-2016-85.

Meier, M.F., and A. Post. 1987. Fast tidewater glaciers. *Journal of Geophysical Research* 92(B9):9,051–9,058, https://doi.org/10.1029/JB092iB09p09051.

Murray, T., N. Selmes, T.D. James, S. Edwards, I. Martin, T. O'Farrell, R. Aspey, I. Rutt, M. Nettles, and T. Baugé. 2015. Dynamics of glacier calving at the ungrounded margin of Helheim Glacier, southeast Greenland. *Journal of Geophysical Research* 120(6):964–982, https://doi.org/10.1002/2015JF003531.

Moon, T., and I. Joughin. 2008. Changes in ice front position on Greenland's outlet glaciers from 1992 to 2007. *Journal of Geophysical Research* 113, F02022, https://doi.org/10.1029/2007JF000927.

Nettles, M., T. Larsen, P. Elósegui, G. Hamilton, L. Stearns, A. Ahlstrøm, J. Davis, M. Andersen, J. de Juan, and S. Khan. 2008. Step-wise changes in glacier flow speed coincide with calving and glacial earthquakes at Helheim Glacier, Greenland. *Geophysical Research Letters* 35, L24503, https://doi.org/10.1029/2008GL036127.

Nick, F.M., A. Vieli, I.M. Howat, and I. Joughin. 2009. Large-scale changes in Greenland outlet glacier dynamics triggered at the terminus. *Nature Geoscience* 2:110–114, https://doi.org/10.1038/ngeo394.

Nick, F.M., C.J. Van der Veen, A. Vieli, and D.I. Benn. 2010. A physically based calving model applied to marine outlet glaciers and implications for the glacier dynamics. *Journal of Glaciology* 56(199):781–794, https://doi.org/10.3189/002214310794457344.

O'Leary, M., and P. Christoffersen. 2013. Calving on tidewater glaciers amplified by submarine frontal melting. *The Cryosphere* 7(1):119–128, https://doi.org/10.5194/tc-7-119-2013.

Otero, J., F.J. Navarro, C. Martin, M.L. Cuadrado, and M.I. Corcuera. 2010. A three-dimensional calving model: Numerical experiments on Johnsons Glacier, Livingston Island, Antarctica. *Journal of Glaciology* 56(196):200–214, https://doi.org/10.3189/002214310791968539.

Parizek, B.R., K. Christianson, S. Anandakrishnan, R.B. Alley, R.T. Walker, R.A. Edwards, D.S. Wolfe, G.T. Bertini, S.K. Rinehart, R.A. Bindschadler, and S.M.J. Nowicki. 2013. Dynamic (in)stability of Thwaites Glacier, West Antarctica. *Journal of Geophysical Research* 118:638–655, https://doi.org/10.1002/jgrf.20044.

Peters, I.R., J.M. Amundson, R. Cassotto, M. Fahnestock, K.N. Darnell, M. Truffer, and W.W. Zhang. 2015. Dynamic jamming of iceberg-choked fjords. *Geophysical Research Letters* 42(4):1,122–1,129, https://doi.org/10.1002/2014GL062715.

Pralong, A., and M. Funk. 2005. Dynamic damage model of crevasse opening and application to glacier calving. *Journal of Geophysical Research* 110, B01309, https://doi.org/10.1029/2004JB003104.

Riesen, P., T. Strozzi, A. Bauder, A. Wiesmann, and M. Funk. 2011. Short-term surface ice motion variations measured with a ground-based portable real aperture radar interferometer. *Journal of Glaciology* 57(201):53–60, https://doi.org/10.3189/002214311795306718.
Rignot, E. 1998. Fast recession of a West Antarctic glacier. *Science* 281(5376):549–551, https://doi.org/10.1126/science.281.5376.549.
Rignot, E., and P. Kanagaratnam. 2006. Changes in the velocity structure of the Greenland Ice Sheet. *Science* 311:986–990, https://doi.org/10.1126/science.1121381.
Rodriguez, E., and J.M. Martin. 1992. Theory and design of interferometric synthetic aperture radars. *IEE Proceedings F (Radar and Signal Processing)* 139(2):147–159, https://doi.org/10.1049/ip-f-2.1992.0018.
Scambos, T., H.A. Fricker, C.C. Liu, J. Bohlander, J. Fastook, A. Sargent, R. Masson, and A.-M. Wu. 2009. Ice shelf disintegration by plate bending and hydro-fracture: Satellite observations and model results of the 2008 Wilkins ice shelf break-ups. *Earth and Planetary Science Letters* 280(1):51–60, https://doi.org/10.1016/j.epsl.2008.12.027.
Schjøth, F., C.S. Andresen, F. Straneo, T. Murray, K. Scharrer, and A. Korablev. 2012. Campaign to map the bathymetry of a major Greenland fjord. *Eos, Transactions American Geophysical Union* 93(14):141–142, https://doi.org/10.1029/2012EO140001.
Schoof, C. 2007. Ice sheet grounding line dynamics: Steady states, stability, and hysteresis. *Journal of Geophysical Research* 112, F03S28, https://doi.org/10.1029/2006JF000664.
Sergeant, A., A. Mangeney, E. Stutzmann, J.P. Montagner, F. Walter, L. Moretti, O. Castelnau. 2016. Complex force history of a calving-generated glacial earthquake derived from broadband seismic inversion. *Geophysical Research Letters* 43:1,055–1,065, https://doi.org/10.1002/2015GL066785.
Shepherd, A., A. Hubbard, P. Nienow, M. King, M. McMillan, and I. Joughin. 2009. Greenland ice sheet daily motion coupled with daily melting in late summer. *Geophysical Research Letters* 36, L01501, https://doi.org/10.1029/2008GL035758.
Strozzi, T., C. Werner, A. Wiesmann, and U. Wegmuller. 2012. Topography mapping with a portable real-aperture radar interferometer. *IEEE Geoscience and Remote Sensing Letters* 9(2):277–281, https://doi.org/10.1109/LGRS.2011.2166751.
Taylor, Z.J., R. Gurka, G.A. Kopp, and A. Liberzon. 2010. Long-duration time-resolved PIV to study unsteady aerodynamics. *IEEE Transactions on Instrumentation and Measurement* 59(12):3,262–3,269.
Timoshenko, S.P., and J.N. Goodier. 1970. *Theory of Elasticity*, 3rd ed. McGraw-Hill, New York, 567 pp.
Truffer, M., and R. Motyka. 2016. Where glaciers meet water: Subaqueous melt and its relevance to glaciers in various settings. *Reviews of Geophysics* 54:220–239, https://doi.org/10.1002/2015RG000494.
Van der Veen, C.J. 1998. Fracture mechanics approach to penetration of surface crevasses on glaciers. *Cold Regions Science and Technology* 27:31–47, https://doi.org/10.1016/S0165-232X(97)00022-0.
Van der Veen, C.J. 2002. Calving glaciers. *Progress in Physical Geography* 26:96–122, https://doi.org/10.1191/0309133302pp327ra.
Vaňková, I., and D.M. Holland. 2016. Calving signature in ocean waves at Helheim Glacier and Sermilik Fjord, East Greenland. *Journal of Physical Oceanography* 46(10):2,925–2,941, https://doi.org/10.1175/JPO-D-15-0236.1.
Vaughan, D.G., and R. Arthern. 2007. Why is it hard to predict the future of ice sheets? *Science* 315:1,503–1,504, https://doi.org/10.1126/science.1141111.
Vieli, A., and F.M. Nick. 2011. Understanding and modelling rapid dynamic changes of tidewater outlet glaciers: Issues and implications. *Surveys in Geophysics* 32(4–5):437–458, https://doi.org/10.1007/s10712-011-9132-4.
Voytenko, D., T.H. Dixon, I.M. Howat, N. Gourmelen, C. Lembke, C.L. Werner, S. De La Peña, and B. Oddsson. 2015a. Multi-year observations of Breiðamerkurjökull, a marine-terminating glacier in southeastern Iceland, using terrestrial radar interferometry. *Journal of Glaciology* 61(225):42–54, https://doi.org/10.3189/2015JoG14J099.
Voytenko, D., A. Stern, D.M. Holland, T.H. Dixon, K. Christianson, and R.T. Walker. 2015b. Tidally driven ice speed variation at Helheim Glacier, Greenland, observed with terrestrial radar interferometry. *Journal of Glaciology* 61(226):301–308, https://doi.org/10.3189/2015JoG14J173.
Walker, C.C., J.N. Bassis, H.A. Fricker, and R.J. Czerwinski. 2015. Observations in the interannual and spatial variability in rift propagation in the Amery Ice Shelf, Antarctica 2002–2014. *Journal of Glaciology* 1(226):243–252, https://doi.org/10.3189/2015JoG14J151.
Walter, J.I., J.E. Box, S. Tulaczyk, E.E. Brodsky, I.M. Howat, Y. Ahn, and A. Brown. 2012. Oceanic mechanical forcing of a marine-terminating Greenland glacier. *Annals of Glaciology* 53(60):181–192, https://doi.org/10.3189/2012AoG60A083.
Weijer, W., M.E. Maltrud, M.W. Hecht, H.A. Dijkstra, and M.A. Kliphuis. 2012. Response of the Atlantic Ocean circulation to Greenland Ice Sheet melting in a strongly-eddying ocean model. *Geophysical Research Letters* 39, L09606, https://doi.org/10.1029/2012GL051611.
Werner, C., T. Strozzi, A. Wiesmann, and U. Wegmuller. 2008. A real-aperture radar for ground-based differential interferometry. Paper presented at the International IEEE Geoscience and Remote Sensing Symposium, July 7–11, 2008, https://doi.org/10.1109/IGARSS.2008.4779320.
Xie, S., T. Dixon, D. Voytenko, D.M. Holland, D. Holland, and T. Zheng. 2016. Precursor motion to iceberg calving at Jakobshavn Isbræ, Greenland, observed with terrestrial radar interferometry. *Journal of Glaciology* 62(236):1,134–1,142, https://doi.org/10.1017/jog.2016.104.

ACKNOWLEDGMENTS

We are grateful to the support provided by the NASA Jet Propulsion Laboratory Oceans Melting Greenland (OMG) grant to DMH at New York University. Additional support from New York University Abu Dhabi through grant G1204 to DMH and DH in the Center for Global Sea Level Change (CSLC) is recognized. The US National Science Foundation provided support to DMH and DH via ARC-1304137, and to BRP via PLR-1443190, ANT-0424589, and AGS-1338832. NASA provided support to BRP via NNX15AH84G and to RTW via NNX12AD03A. Air Greenland is acknowledged for providing superb helicopter support over the glacier, Brian Rougeux for field safety operations, and Captain Sigurdur Petursson for ocean tasks.

AUTHORS

David M. Holland (david.holland@nyu.edu) is Professor, Courant Institute of Mathematical Sciences, New York University, New York, NY, USA, and Center for Global Sea Level Change, NYU Abu Dhabi, Abu Dhabi, UAE. **Denis Voytenko** is Postdoctoral Associate, Courant Institute of Mathematical Sciences, New York University, New York, NY, USA. **Knut Christianson** is Assistant Professor, Department of Earth & Space Sciences, University of Washington, Seattle, WA, USA. **Timothy H. Dixon** is Professor, School of Geosciences, University of South Florida, Tampa, FL, USA. **M. Jeffrey Mei** is PhD student, MIT-WHOI Joint Program in Oceanography, Woods Hole, MA, USA, and Cambridge, MA, USA. **Byron R. Parizek** is Assistant Professor, Mathematics & Geoscience, The Pennsylvania State University, DuBois, PA, USA. **Irena Vaňková** is PhD student, Courant Institute of Mathematical Sciences, New York University, New York, NY, USA, and Center for Global Sea Level Change, NYU Abu Dhabi, Abu Dhabi, UAE. **Ryan T. Walker** is Assistant Research Scientist, Earth System Science Interdisciplinary Center, University of Maryland, College Park, MD, USA. **Jacob I. Walter** is Research Associate, Institute for Geophysics, University of Texas at Austin, Austin, TX, USA. **Keith Nicholls** is Oceanographer, British Antarctic Survey, Cambridge, UK. **Denise Holland** is Field and Logistical Manager, Courant Institute of Mathematical Sciences, New York University, New York, NY, USA, and Center for Global Sea Level Change, NYU Abu Dhabi, Abu Dhabi, UAE.

ARTICLE CITATION

Holland, D.M., D. Voytenko, K. Christianson, T.H. Dixon, M.J. Mei, B.R. Parizek, I. Vaňková, R.T. Walker, J.I. Walter, K. Nicholls, and D. Holland. 2016. An intensive observation of calving at Helheim Glacier, East Greenland. *Oceanography* 29(4):46–61, https://doi.org/10.5670/oceanog.2016.98.